ACS APPLIED MATERIALS & INTERFACES

Research Article

Cite This: ACS Appl. Mater. Interfaces 2018, 10, 26641−26652

www.acsami.org

Downloaded via HONG KONG UNIV SCIENCE TECHLGY on July 11, 2019 at 08:34:28 (UTC).
See https://pubs.acs.org/sharingguidelines for options on how to legitimately share published articles.

Graphene/Boron Nitride−Polyurethane Microlaminates for Exceptional Dielectric Properties and High Energy Densities

Ying Wu,[†] Zhenyu Wang,[†] Xi Shen,[†] Xu Liu,[†] Ne Myo Han,[†] Qingbin Zheng,[†,‡] Yiu-Wing Mai,[§] and Jang-Kyo Kim*,[†]

[†]Department of Mechanical and Aerospace Engineering, [‡]Institute for Advanced Study, The Hong Kong University of Science and Technology, Clear Water Bay, Kowloon, Hong Kong

[§]Centre for Advanced Materials Technology, School of Aerospace, Mechanical and Mechatronic Engineering, University of Sydney, Sydney, NSW 2006, Australia

Supporting Information

ABSTRACT: Hexagonal boron nitride (h-BN) has tremendous potential for dielectric energy storage by rationally assembling with graphene. We report the fabrication of microlaminate composites consisting of alternating reduced graphene oxide (rGO) and h-BN nanosheets embedded in a polyurethane (PU) matrix using a novel, two-step bidirectional freeze casting process. Porous, highly-aligned rGO−PU aerogels having ultrahigh dielectric constants with relatively high dielectric losses and low dielectric strengths are fabricated by initial freeze casting. The losses are suppressed, whereas the dielectric strengths are restored by assembling the porous rGO−PU skeleton with electrically insulating BN−PU tunneling barrier layers in the second freeze casting routine. The ligaments bridging the conductive rGO−PU layers are effectively removed by the BN−PU barrier layers, eliminating the current leakage in the transverse direction. The resultant rGO−PU/BN−PU microlaminate composites deliver a remarkable dielectric constant of 1084 with a low dielectric loss of 0.091 at 1 kHz. By virtue of synergy arising from both the rGO−PU layers with a high dielectric constant and the BN−PU barrier layers with a high dielectric strength, the microlaminate composites present a maximum energy density of 22.7 J/cm^3, 44 folds of the neat rGO−PU composite acting alone. The promising overall dielectric performance based on a microlaminate structure offers a new insight into the development of next-generation dielectric materials.

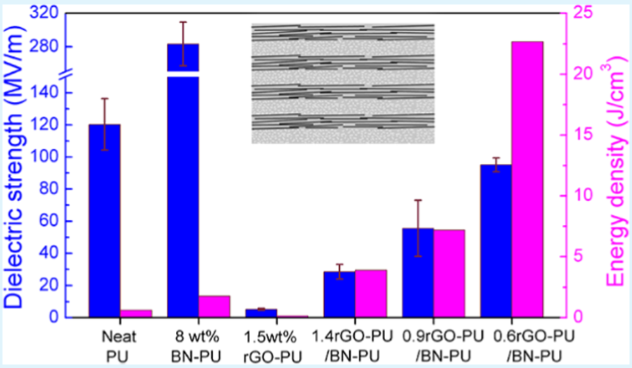

KEYWORDS: *reduced graphene oxide, boron nitride, microlaminates, dielectric properties, energy density*

1. INTRODUCTION

The rapid advances in the design, integration, and miniaturization of modern electronics reply on the performance of dielectric capacitors, which exhibit extremely fast charge and discharge characteristics. Unlike supercapacitors and batteries, dielectric capacitors show negligible performance degradation during services, ensuring their super-long lifetime. In general, the intrinsic performance of a capacitor is characterized by the stored energy density, U, which is determined by

$$U = \int E \, \mathrm{d}D \tag{1}$$

where E and D are the applied electric field and the electric displacement, respectively.[1] The maximum stored energy density, $U_{\max}$, of a capacitor is quantified by[2,3]

$$U_{\max} = 0.5\varepsilon_0\varepsilon_r E_b{}^2 \tag{2}$$

where ε_0, ε_r, and E_b are the permittivity of vacuum (=8.854 × 10^{-12} F/m), the dielectric constant and the dielectric strength of the material, respectively. The $U_{\max}$ is also a representation of the maximum charge energy density. Therefore, besides a high dielectric constant and a low dielectric loss, a high dielectric strength is another critical parameter that should be taken into account when designing superior dielectric materials with high energy densities.

Conductive fillers and ceramics with high dielectric constants (high-k) are the most popular reinforcements for the development of high-k polymer-based composites. Nanocarbon materials, such as carbon nanotubes (CNTs) and graphene, are effective fillers for enhanced dielectric constants due to the interfacial polarization arising from the large difference in conductivity between the carbon fillers and the insulating polymer matrices. A dielectric constant as high as over 10 000 at 1 kHz has been reported for reduced graphene

Received: May 16, 2018
Accepted: July 11, 2018
Published: July 11, 2018

© 2018 American Chemical Society

DOI: 10.1021/acsami.8b08031

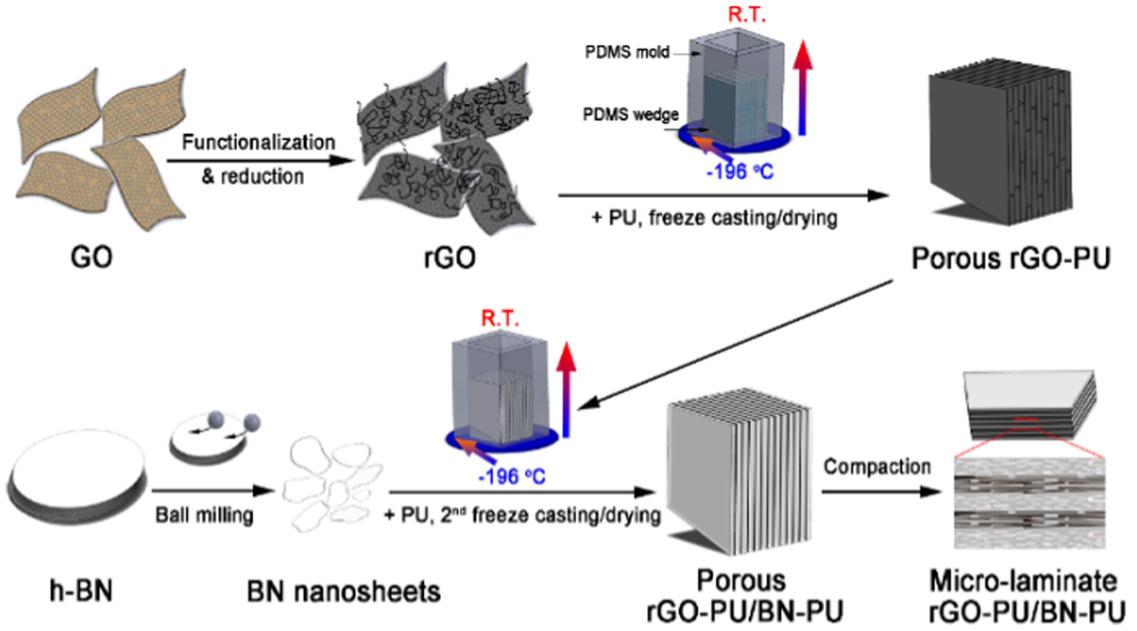

Figure 1. Schematic procedure of the synthesis of highly aligned rGO−PU/BN−PU microlaminate composites.

oxide (rGO)/epoxy composites,[4] but their dielectric loss and dielectric strength were unsatisfactory for practical applications because they suffer from the inevitably high leakage currents after the incorporation of conductive fillers. High-*k* ceramics, such as calcium copper titanate ($CaCu_3Ti_4O_{12}$), lead zirconate titanate ($Pb[Zr_xTi_{1-x}]O_3$ ($0 \leq x \leq 1$)), and barium titanate ($BaTiO_3$), greatly enhanced the dielectric constants with marginal sacrifice of slightly increased losses.[5−7] However, a large amount of ceramic fillers is often needed to achieve high dielectric constants, inevitably deteriorating the mechanical properties and the dielectric strengths of the composites because of the defects generated at such high filler contents.

Several approaches have been proposed to address the foregoing issues so that both the dielectric constant and the dielectric strength are simultaneously enhanced to improve the energy density of the material. The following strategies are considered promising, including (i) the encapsulation of conductive fillers by insulating materials,[8−10] (ii) the incorporation of high-E_b fillers,[11−13] and (iii) the combination of high-*k* (conductors or ceramics) and high-E_b materials.[1,14] The first strategy has been achieved by in situ polymerization or growth of insulating polymers or inorganic particles on conductive filler surface, so that the direct interconnection of conductive additives was prevented, which in turn mitigated the dielectric loss and improved the dielectric strength by suppressing leakage currents.[8−10] The addition of fillers with intrinsically high-E_b is effective for the improvement of dielectric performance. Boron nitride (BN) nanosheets obtained by exfoliation of hexagonal BN (h-BN) were proven to be particularly promising for the enhancement of energy densities and the reliability of dielectrics.[11−13] For example, the BN/poly(vinylidene fluoride-ter-trifluoroethylene-ter-chlorofluoroethylene) (P(VDF-TrFE-CFE)) composite delivered an energy density of more than 2-folds of the neat P(VDF-TrFE-CFE),[11] although there was a marginal reduction in dielectric constant after the addition of BN. Three-layer sandwich structures were introduced to take full advantages of high dielectric constants of high-*k* fillers and high dielectric strengths of ceramics.[1,14] The layered structure was confirmed to be more effective in blocking conductive paths and suppressing leakage currents than simple mixing of high-*k* and high-E_b fillers.[14] Although several studies covering the synergistic effects of high-*k* ceramics and high-E_b BN on dielectric properties have been reported,[1,14] the collaborative contributions of conductive and high-E_b fillers are rare.

With the foregoing studies in mind, we developed microlaminate composites comprising alternating rGO−polyurethane (PU) and BN−PU layers (Figure 1) in this study to simultaneously offer high dielectric constants, low dielectric losses, and high energy densities. Solid rGO−PU/BN−PU microlaminate composites were fabricated using a novel, two-step bidirectional freeze casting and drying process, where the aligned porous rGO−PU aerogel skeleton was infiltrated by a BN−PU aqueous suspension, followed by compaction. This is the first report on developing a microlaminar structure consisting of both high-*k* and high-E_b laminates. The high-*k* rGO−PU laminates with relatively high dielectric losses were spatially separated by the low-loss, high-E_b rGO−PU layers, simultaneously achieving reduced dielectric losses and enhanced dielectric strengths. The composites delivered an ultrahigh dielectric constant of 1084 and a low dielectric loss of 0.091 along with a remarkable U_{max} of 22.7 J/cm^3, which is 37-folds of the neat PU.

2. EXPERIMENTAL SECTION

2.1. Synthesis of Aligned Porous rGO−PU Aerogels. Graphene oxide (GO) was prepared by the modified Hummers method,[15,16] and the typical size distribution of GO sheets is shown in Figure S1. The GO sheets were functionalized using polydopamine by in situ polymerization of dopamine monomers because of its excellent affinity to both GO and organic matrix materials.[17] Fifty milligrams of GO dispersion was diluted in 200 mL of deionized (DI) water, followed by the addition of 10 mM Trizma base (supplied by Sigma). The pH value of the solution was adjusted to 8.5 using ammonia solution (supplied by Uni-chem), followed by the addition of 150 mg dopamine hydrochloride (supplied by Sigma). The mixture was kept at 70 °C for 24 h for in situ polymerization of polydopamine on the GO sheets and the treated GO was washed with DI water several times to remove superfluous polydopamine. The resultant product

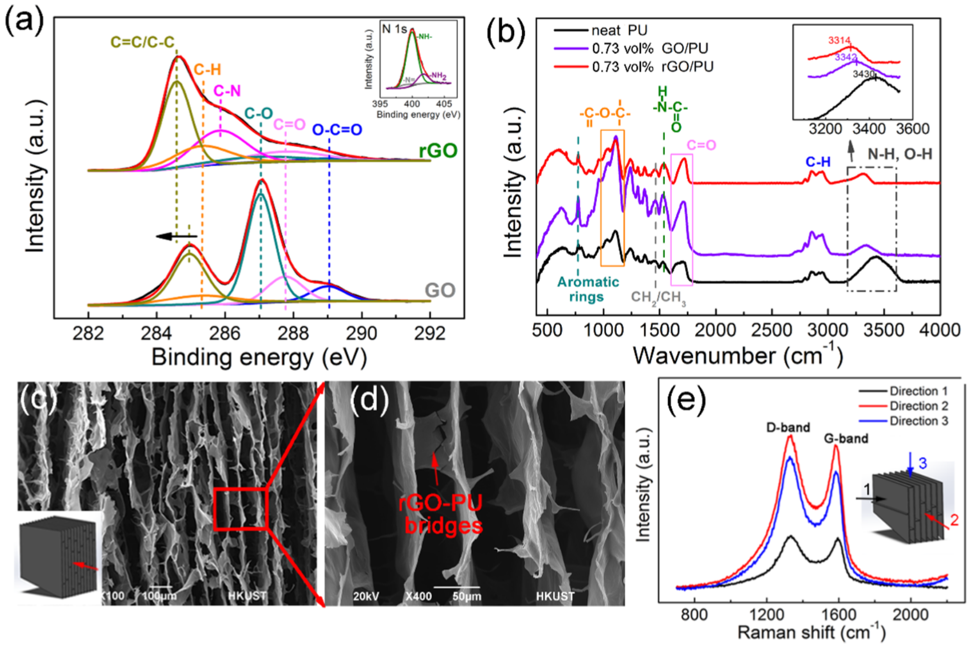

Figure 2. (a) Deconvoluted C 1s XPS spectra of GO and rGO after functionalization and reduction with deconvoluted N 1s spectrum in inset. (b) FT-IR of neat PU, GO−PU, and rGO−PU composites, showing enhanced interfacial interactions after the functionalization and reduction of GO with magnified peaks in inset. (c, d) Side-view SEM images of porous rGO−PU composites at different magnifications. (e) Raman spectra of porous rGO−PU composites measured in different directions as indicated in inset.

was reduced by hydrazine (Aldrich, 35 wt % in water) at 90 °C overnight at a hydrazine-to-GO weight ratio of 3:1. The rGO dispersion was blended with waterborne PU emulsion (NeoRez R-600 supplied by DSM NeoResin) and sonicated for 1 h to obtain a homogeneous solution. The waterborne PU was employed as the matrix because of its water dispersive characteristic and high flexibility, making the freeze-casting/drying and the compaction (as described below) process possible. The rGO−PU dispersion was freeze-cast using a custom-made apparatus, where the unidirectional freeze-casting tool developed previously[18] was modified to achieve bidirectional freeze casting. The bottom part of casting mold was replaced by a poly(dimethyl siloxane) (PDMS) wedge similar to a recent report[19] to allow simultaneous casting in two orthogonal directions. The details of the bidirectional freeze-casting apparatus are shown in Figure S2. The freeze-cast rGO−PU hydrogel was subsequently freeze-dried (SuperModulyo, Thermo Fisher) at −70 °C for 48 h to obtain aligned, porous rGO−PU aerogels, which were used as the skeleton for the preparation of rGO−PU/BN−PU microlaminate composites.

2.2. Fabrication of rGO−PU/BN−PU Microlaminate Composites. The h-BN flakes were exfoliated by a urea-assisted ball-milling method with an h-BN/urea weight ratio of 1:60 at 400 rpm for 24 h on a planetary ball mill (QM-3SP2). The application of urea was proven to be effective in assisting exfoliation and protecting the BN nanosheets from excessive mechanical damage to their lattice structure.[20] The ball-milled powders were dispersed in DI water for centrifugation at 4000 rpm for 2 h to collect the supernatant, which was washed with DI water several times to remove the residual urea and freeze-dried to obtain the BN nanosheets. The BN−PU films with different BN contents were fabricated by drop casting for the measurements of dielectric strengths. The suspensions containing different solid concentrations of BN−PU were infiltrated into the aligned porous rGO−PU aerogels in a vacuum oven, followed by a second freeze-casting and freeze-drying routine. The resulting flexible, porous rGO−PU/BN−PU composites were compacted by pressing at ∼10 MPa to form solid, highly-aligned rGO−PU/BN−PU microlaminate composites with alternating rGO−PU and BN−PU layers. The composites were designated as rGO−PU/BN−PU_*X*, where *X* is the volume ratio of rGO−PU to BN−PU laminates in composites. The volumetric fractions were calculated using the densities of 2.2, 2.3, and 1.06 g/cm^3 for rGO, BN nanosheets, and PU according to the suppliers' specifications, respectively. The schematic of the above fabrication procedure is illustrated in Figure 1.

2.3. Characterization. The elemental compositions and chemical structure of GO before and after the reduction were examined by X-ray photoelectron spectroscopy (XPS, Axis Ultra DLD). The dispersion of rGO sheets in the PU matrix and the exfoliation of h-BN were characterized on an X-ray diffraction analyzer (XRD, PANalytical X'pert Pro) using Cu $K\alpha_1$ (λ = 0.154 nm) radiation. Morphologies of different composites were examined on a scanning electron microscope (SEM, JEOL JSM 6390). The size distribution and thickness measurement of BN nanosheets were conducted using a SEM, a transmission electron microscope (TEM, JEOL JEM 2010), and an atomic force microscope (AFM, NanoScope IIIa/Dimension 3100). Raman spectroscopy (Reinshaw MicroRaman/Photoluminescence System) was used to examine the structural change of BN before and after exfoliation. The functional groups on BN, the chemical bonds of GO before and after functionalization and reduction, and the interfacial interactions between rGO and PU were studied by Fourier transform infrared spectroscopy (FT-IR, Bruker Vertex 70Hyperion 1000). The dielectric properties of solid rGO−PU composites and rGO−PU/BN−PU microlaminate composites with different filler contents were studied on an impedance/gain-phase analyzer (Hewlett Packard 4149A) in the frequency range from 100 Hz to 40 MHz. The dielectric strength was measured on a ferroelectric analyzer (TF Analyzer 2000E).

3. RESULTS AND DISCUSSION

3.1. Reduction of GO and Dielectric Properties of rGO−PU Composites.

The general XPS spectrum (Figure S3a) of rGO presents a prominent N 1s peak at 400 eV as a reflection of functionalization by polydopamine and reduction by hydrazine, both of which were absent in GO. After the functionalization and reduction, the intensity of O 1s of rGO significantly reduced. Consequently, the atomic C/O ratios of rGO (inset table in Figure 2a) increased from 1.38 to 4.3, which was lower than those of rGO reported in the literature[18,21] because of the presence of O atoms in the

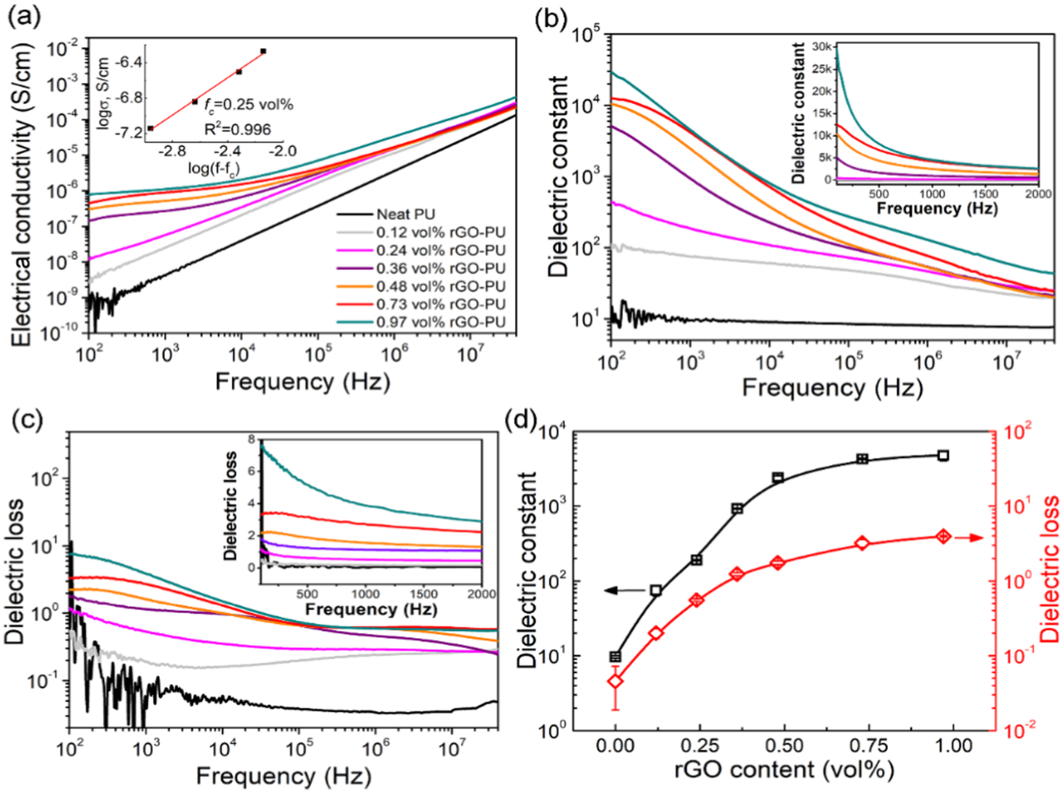

Figure 3. Dielectric properties of rGO−PU composites with different filler contents: (a) alternating current (AC) conductivity, (b) dielectric constant, (c) dielectric loss, and (d) summary of dielectric performance at 1 kHz. Insets in (a)−(c) are the percolation threshold obtained according to the power law; and the dielectric constant and dielectric loss of composites plotted in linear scales within a frequency range of 100−2000 Hz, respectively.

polydopamine chains. The deconvoluted C 1s spectra of GO (Figure 2a) consisted of C═C/C−C (284.9, eV), C−H (285.3 eV), C−O (287 eV), C═O (287.8 eV), and O−C═O (289 eV) functional groups.[22] After the functionalization and reduction, a new peak appeared at 285.8 eV, corresponding to C−N in rGO, whereas the intensities of oxygenated functional groups were significantly reduced. The C═C/C−C peak of rGO underwent an obvious downshift after the reduction, as indicated by the black arrow, suggesting the formation of $\pi-\pi$ stacking between the graphitic units of rGO sheets and the aromatic rings of polydopamine.[23] A comparison of deconvoluted C 1s spectra of the polydopamine-functionalized GO before and after reduction is given in Figure S3b. The GO sheets were partially reduced by the amine functional groups in polydopamine chains,[17,24] showing significantly reduced intensities of C−O and O−C═O peaks. After the hydrazine treatment, the functionalized GO sheets were further reduced with weakened oxygen-containing groups, especially the C−O and C═O species. The deconvoluted N 1s spectrum of rGO showed a predominant N−H (400 eV) peak and two minor peaks of −N═ (389.9 eV) and $-\mathrm{NH_2}$ (401.7 eV) functional groups (inset in Figure 2a).

In spite of the largely different chemical nature of GO before and after functionalization and reduction, both GO−PU and rGO−PU composites presented similar FT-IR spectra to the neat PU. The peptide bond peak of PU located at 1530 cm^{-1} shifted to 1535 cm^{-1} after the incorporation of GO sheets, indicating strong interactions between the peptide bonds in PU chains and the oxygenated groups in GO sheets. The peak position underwent a further shift to 1537 cm^{-1} in the polydopamine-functionalized rGO, a suggestion of enhanced interfacial interactions as the long tails of wrapped polydopamine on GO sheets likely penetrated into the PU molecules.[25] The broad peak at ~3400 cm^{-1}, a representation of N−H/O−H stretching vibration, exhibited an obvious downshift, indicating the formation of strong hydrogen bonds between the oxygenated functional groups on the GO sheets and the PU matrix.[26] With the incorporation of the polydopamine-functionalized rGO, much stronger hydrogen bonds were expected as indicated by the extended downshift of the peak position (inset in Figure 2b), attributed to the large amount of oxygen- and nitrogen-containing groups in polydopamine and the polydopamine chains penetrating into the PU matrix as discussed above. The XRD pattern of GO had a peak at 2θ = 7.7° (Figure S3c), reflecting a *d*-spacing of 1.15 nm, which is much larger than that of pristine graphite as a result of intercalation of high concentration acid into the GO layers.[15,16] The 0.73 vol % rGO−PU composites presented an XRD pattern very similar to that of the neat PU with a characteristic peak at 19.5°, showing the absence of the characteristic peak of the GO sheets at 7.7°. This signified the uniform dispersion of polydopamine-functionalized rGO sheets in the matrix with enhanced interfacial interactions.

The morphologies and structures of the rGO−PU composites before compaction were examined by SEM and Raman spectroscopy, as shown in Figure 2c−e. The porous state of rGO−PU composites obtained after freeze-casting and drying process[27] presented highly aligned longitudinal skeleton, which is intermittently connected by transverse bridges (Figure 2c,d). The bidirectional freeze casting produced a highly oriented rGO−PU composites in the two orthogonal directions (Figure S4a). The SEM image of freeze-fractured surface (Figure S4b) indicates that the composites consisted of large pieces of rGO−PU laminates (as indicated by white arrows) interconnected by rGO−PU bridges. These SEM images taken from different directions (Figures 2c,d and S4) confirmed that a highly aligned layered structure was formed owing to the bidirectional temperature gradients generated using the PDMS wedge. The large temperature gradients along the two directions, namely from the mold bottom to the top surface and along the slope of PDMS wedge (Figure S2), resulted in the nucleation of ice crystals at the thinnest edge of the PDMS wedge and their laminar growth directed by the dual temperature gradients (Figure S5a,i). Without the PDMS wedge, the ice crystals tended to nucleate randomly at the bottom of the mold, leading to only longitudinal alignment of rGO−PU composites (Figure S5b,iii).[19]

The polarized Raman spectroscopy has been widely used to study the alignment of carbon materials, such as CNTs and graphene.[21,28,29] The intensities of Raman bands of these carbon allotropes are highly sensitive to the relative direction of the polarized incident laser, exhibiting the most intensified peaks when the laser light is aligned along the alignment direction while obtaining the most suppressed bands with incident laser oriented perpendicular to it.[18] The Raman spectra of porous rGO−PU composites exhibited two major peaks (Figure 2e), the D- and G-bands, reflecting disordered sp^3 hybridization and the doubly degenerate zone center E_{2g} mode, respectively. The intensities of these peaks for the porous rGO−PU composites were largely different along the three major directions. Much higher intensities were observed in the directions 2 and 3 than in the direction 1, signifying the orientation of rGO sheets in the composites along these two directions. With the incident laser oriented transverse to the alignment direction (direction 1 in Figure 2e), the intensities of the Raman peaks were significantly suppressed, suggesting lack of alignment, which is consistent with the SEM morphologies. Apart from the good alignment arising from the bidirectional freeze-casting, the large size GO precursors (Figure S1) also enhanced the alignment, contributing to high dielectric constants of the rGO−PU composites (Figure 3d).[4]

The alternating current (AC) conductivities and dielectric properties of solid rGO−PU composites containing different filler contents obtained after compaction are shown in Figure 3a−d. The AC electrical conductivity of composites significantly enhanced with increasing rGO content (Figure 3a), indicating effective reduction of the GO sheets. The AC conductivities of composites reinforced with conductive fillers can be expressed using a resistance−capacitance percolation model. The model includes a frequency-independent Ohmic conductivity attributed to the migration of charge carriers and a frequency-dependent capacitive conductivity owing to the dielectric component.[30] Both neat PU and composites with low filler contents (≤0.24 vol %) showed a linear relationship with frequency in a log−log plot, typical of those below percolation threshold.[31] No conducting network was formed, typical of a frequency-dependent capacitor-like behavior. However, the composites with higher rGO contents (≥0.36 vol %) exhibited a plateau in conductivity at a low frequency region below 10 kHz, showing conductivities dominated by a frequency-independent Ohmic characteristic because of the formation of percolating networks. At high frequencies, they exhibited capacitive electrical conductivities. The percolation threshold of composites, f_c, was calculated following the power law equation[32]

$$\sigma = \sigma_f (f - f_c)^n \tag{3}$$

where σ is the electrical conductivity of the composites, σ_f is the conductivity of the filler, f is the filler content, and n is the critical exponent. The log−log relationship of σ and $(f - f_c)$ (see the inset in Figure 3a) gave a percolation threshold of 0.25 vol % for the rGO−PU composites.

The dielectric constant of rGO−PU composites greatly improved with increasing filler content, especially at filler contents above the percolation threshold at low frequencies (Figure 3b). This is attributed to the significantly enhanced interfacial polarization at high rGO contents, arising from the large disparity in electrical conductivity between the conductive fillers and the insulating PU matrix.[31,33] The polarized charges generated from the conductive fillers upon the application of external electric field gather around the rGO/PU interfaces, naturally forming numerous micro- or nanocapacitors. The contributions of fillers for the formation of nanocapacitors and thus the enhancement of dielectric constant were maximized if the rGO sheets were highly aligned.[4] However, the transversely interconnected rGO sheets were detrimental to the dielectric loss, giving rise to increased dielectric losses with increasing filler contents (Figure 3c). Leakage currents sharply increased when rGO conductive networks were formed at filler contents above the percolation threshold.[34]

The dielectric properties of rGO−PU composites determined at a reference frequency of 1 kHz are summarized in Figure 3d. The highest dielectric constant of 4759 was obtained at 0.97 vol % rGO at the expense of a large dielectric loss of 3.9. A comparison is made of dielectric properties among the current rGO−PU composites and other composites reinforced with different conductive fillers (Figure S6a). The rGO−PU composites exhibited both high dielectric constants with moderately high dielectric losses, which are attributed to (i) the strong interfacial polarization arising from the highly conductive nature of well-reduced rGO sheets and (ii) suppressed polarization relaxation due to strong interfacial interactions arising from the polydopamine functionalization. Taking advantage of the high dielectric constants, balanced dielectric properties with significantly reduced losses were achieved after the second freeze-casting/drying routine, as discussed below. With increasing filler content, dielectric strengths of the composites decreased sharply from 120 MV/m of the neat PU to 5 MV/m of 0.97 vol % rGO−PU composites (Figure S6b) as a result of the much increased leakage currents. This means that a high dielectric constant and a low dielectric loss or a high dielectric strength of conducting filler composites are mutually exclusive, and one property can only be tailored at the expense of the other.

A further study was made in an effort to simultaneously achieve high dielectric constants, low dielectric losses, high dielectric strengths, and high energy densities. For this purpose, the porous 0.73 vol % rGO−PU composite with the highest dielectric constant/loss ratio (Figure S6b) among all rGO−PU composites was chosen for further optimization. The dielectric constant/loss ratio or "dielectric ratio" has been considered a measure of overall dielectric performance of materials.[35] Insulating BN−PU layers with high dielectric

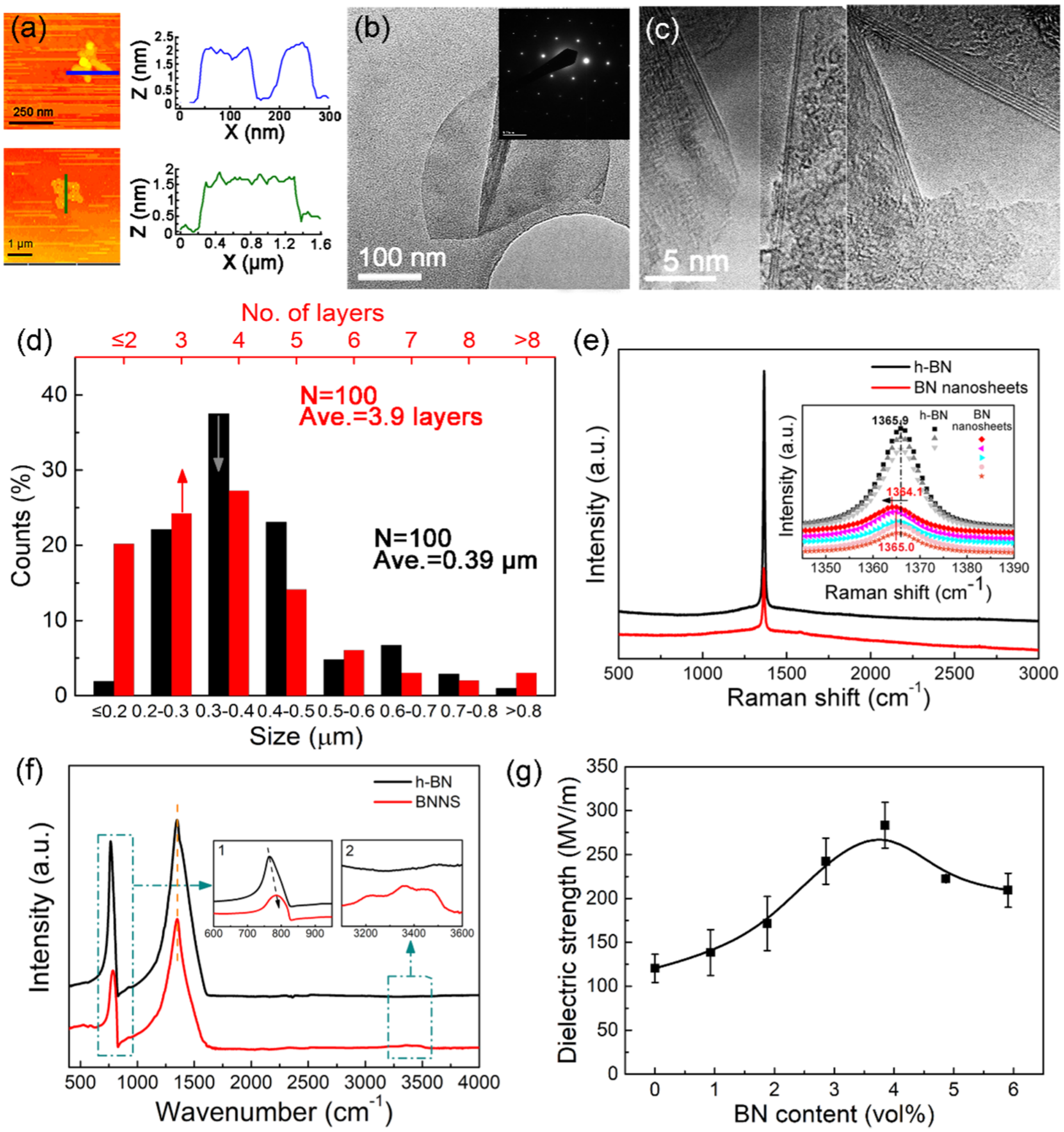

Figure 4. (a) AFM images and corresponding height profiles, (b) TEM and (c) high-resolution TEM images, and (d) distributions of size and number of layers of BN nanosheets. (e) Raman spectra of h-BN and exfoliated BN nanosheets. (f) FT-IR of h-BN flakes and BN nanosheets. (g) Dielectric strengths of BN−PU composites as a function of BN content. Insets in (b) and (f) are the SEAD pattern of BN nanosheets and the magnified curves of selected regions, respectively.

strengths were introduced among the high-*k* 0.73 vol % rGO−PU layers to form a microlaminate structure.

3.2. Exfoliation of h-BN and Dielectric Strength of BN−PU Films. Several methods have been developed for the exfoliation of h-BN—such as liquid phase exfoliation, chemical assisted exfoliation, gas exfoliation, electrochemical exfoliation, and ball milling[20,36−38]—among which the ball-milling method is proven to give effective exfoliation with the highest yields of h-BN nanosheets. In this study, the h-BN flakes (Figure S7a) were exfoliated by urea-assisted ball milling. Urea molecules were adsorbed and intercalated into the BN layers during ball milling, resulting in enhanced interlayer spacing to allow exfoliation of the BN sheets.[20] The SEM images of exfoliated BN nanosheets (Figure S7b) on a SiO_2/Si substrate showed a similar contrast difference to the GO sheets deposited on the same substrate,[15] a typical characteristic of exfoliated two-dimensional materials with single or a few layers. The dark area demonstrates effective exfoliation of the BN flakes into the h-BN nanosheets. The AFM height profiles present nanosheet thicknesses of 1.7−2.0 nm (Figure 4a), equivalent to 3−4 layers,[39,40] taking into account the solvent residue entrapped between the BN sheets and the underlying substrate, although the *d*-spacing of h-BN is 3.3 Å.[41] The TEM images present well-exfoliated BN nanosheets (Figure 4b,c) with a crystalline structure, which is indicated by the selected area electron diffraction (SEAD) pattern (inset of Figure 4b). The h-BN nanosheets exfoliated by the urea-assisted method had an average lateral size of 0.39 *μ*m and an average number of 3.9 layers (Figure 4d). The h-BN sheets were inevitably fragmented into smaller pieces because of the high-energy ball impacts. It is reported that an ultrasmall thickness of the BN sheets was essential for the high dielectric strengths of the BN/polymer composites. However, the dielectric strength became almost insensitive to lateral size of the BN nanosheets ranging from 0.25 to 0.4 *μ*m when they had an average layer number of ~4.[11] Therefore, the BN nanosheets applied in this study achieved excellent dielectric strengths, indicating a moderate size effect of the BN sheets.

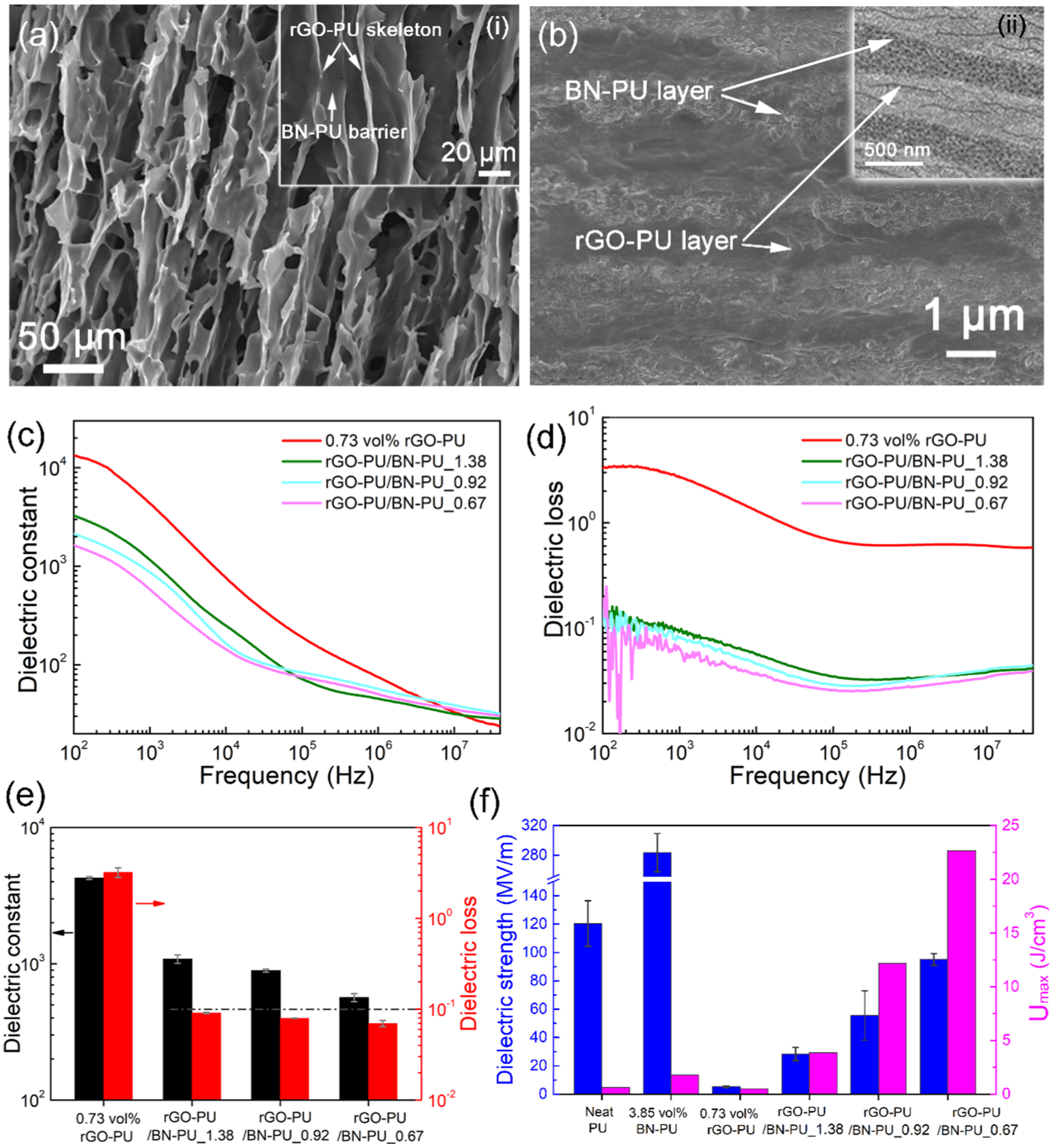

Figure 5. SEM images of (a) porous and (b) solid rGO−PU/BN−PU microlaminate composites before and after compaction, respectively; (c) dielectric constant and (d) dielectric loss vs frequency; (e) summary of dielectric properties at 1 kHz; and (f) dielectric strength and maximum stored energy density of PU, rGO−PU, BN−PU, and rGO−PU/BN−PU composites. Insets (i) and (ii) are the magnified SEM image of porous rGO−PU/BN−PU and the TEM image of the solid rGO−PU/BN−PU composites, respectively.

The XRD patterns of h-BN flakes and BN nanosheets are shown in Figure S7c. No urea peaks were observed in the pattern of BN nanosheets, confirming complete removal of urea after centrifugation. The h-BN's major characteristic peak centered at 21.7° corresponds to the (002) plane, which remained strong as the preferential plane for BN after exfoliation, reflecting the relatively weak interlayer bond among the (002) planes.[41] The intensities of the other peaks at 42.1 and 55.4°, representing the (100) and (004) planes of BN, respectively, significantly reduced compared to those of h-BN because of the medium bonding energy. Several weak diffraction peaks at 44.1, 50.3, 76.3, and 82.5° correspond to the (101), (102), (110), and (112) plane in h-BN, respectively. They disappeared in BN nanosheets, reflecting high bonding energies of these planes. The Raman spectra of both h-BN flakes and BN nanosheets exhibited a characteristic peak at ~1365 cm^{-1}, and the intensity significantly reduced after exfoliation from h-BN to BN nanosheets, see Figure 4e. The full width at half-maximum of these peaks increased from 9.4 cm^{-1} for h-BN flakes to 11.8 cm^{-1} for BN nanosheets because of a stronger surface scattering after exfoliation.[42] Analogous to graphite and graphene, the Raman peak position is proven to be sensitive to the number of layers of BN. The peak position underwent an upshift when the number of BN layers reduced from the bulk h-BN flakes to monolayer BN due to the hardening of E_{2g} phonon mode induced by a slightly shorter B−N bond in the isolated monolayer BN.[43] It is proposed previously that the peaks of double- and few-layer BN sheets shifted downward due to the random strains induced during cleavage or exfoliation, whereas BN sheets thicker than 10 layers presented almost the identical peak position to that of bulk h-BN.[42] The comparison of the characteristic peak at

1365.9 cm^{-1} between the h-BN flakes and the BN nanosheets (inset of Figure 4e) clearly downshifted, demonstrating exfoliation of the BN sheets to less than 10 layers.

The FT-IR spectra in Figure 4f show that both h-BN flakes and BN nanosheets had prominent peaks at ~770 and 1350 cm^{-1}, corresponding to the in-plane B−N−B stretching vibrations and the out-of-plane B−N bending vibrations, respectively.[44] The former peak upshifted from 765.7 to 783.0 cm^{-1} after exfoliation, possibly because of the wrinkles generated in the thin BN nanosheets. A new broad band of the N−H stretching vibrations appeared in the BN nanosheets, a reflection of functionalization of BN by urea during the ball-milling process. The functionalization of the BN nanosheets using urea-assisted ball milling has been studied previously.[20] The high-energy ball collisions led to mechanochemical reaction where the amino groups were chemically bonded with edges and physically adsorbed onto the B sites of the BN nanosheets.

BN−PU composite films were prepared by drop casting and their dielectric strengths were measured, as shown in Figure 4g. The dielectric strength enhanced drastically from 120 MV/m to a maximum value of 283 MV/m at a BN content of 3.85 vol %. With further increase in the filler content, the dielectric strength suffered a downward trend possibly due to agglomeration of the fillers. Therefore, the 3.85 vol % BN−PU composite was chosen for the fabrication of rGO−PU/BN−PU microlaminate composites to study their dielectric properties and energy densities.

3.3. Dielectric Properties of rGO−PU/BN−PU Microlaminate Composites. BN nanosheets, of 3.85 vol %, were mixed with PU suspension and diluted with DI water before infiltration into the aligned porous rGO−PU aerogels in the second freeze-casting routine, followed by freeze-drying. The resultant rGO−PU/BN−PU microlaminate composites before and after compaction are shown in Figure 5a,b, respectively. The aligned skeleton of conductive rGO−PU composite layers remained intact through which the insulating BN−PU barriers were intercalated (Figure 5a). After compaction, the conductive rGO−PU layers were separated by the electrically insulating BN−PU layers in the solid rGO−PU/BN−PU composites, forming a microlaminate structure with uniformly distributed alternating rGO−PU and BN−PU layers of thicknesses ranging from 200 to 1000 nm (Figure 5b). In contrast to the unidirectional freeze-casting method, which has been widely used to fabricate aligned structure in the longitudinal direction,[18,19,35] the bidirectional freeze casting led to a microlaminate structure that is more effective in blocking conductive paths in the thickness direction (Figure S5a,ii) than the structure with random cross-sectional configuration (Figure S5b,iv). The aligned rGO sheets observed in the rGO−PU layers (inset (ii) in Figure 5b) functioned as the nanoscale capacitors, giving rise to high dielectric constants.[4] It is well known that a high dielectric loss is directly related to the interconnected conductive materials, whereas a high dielectric strength has an inverse relationship with it. Therefore, the separation of the conductive rGO−PU skeleton by the insulating BN−PU barriers in the microlaminate composites is expected to result in lower dielectric losses and higher dielectric strengths.

The frequency-dependent dielectric properties of rGO−PU and rGO−PU/BN−PU composites are shown in Figure 5c,d. As expected, both dielectric constant and dielectric loss of rGO−PU/BN−PU composites were lower than those of the 0.73 vol % rGO−PU composite over the whole frequency range studied. The positive effect of the BN−PU barrier layers on reducing dielectric loss was particularly encouraging, which is attributed to the significantly suppressed tunneling currents among electrically conductive rGO−PU layers. The AC conductivities of PU (Figure S7a) decreased with the addition of 3.85 vol % BN nanosheets due to the formation of insulating BN networks, which acted as an efficient barrier against the space−charge conduction and the leakage current.[11] After introducing the highly insulating BN−PU barrier layers among the conductive rGO−PU layers, the electrical conduction among the rGO−PU layers was effectively mitigated, resulting in significantly reduced AC conductivities of the microlaminate composites compared to the rGO−PU composites (Figure S8b). Unlike the 0.73 vol % rGO−PU composites, the rGO−PU/BN−PU microlaminate composites showed capacitor-like AC conductivities over the whole frequency range, indicating broken percolation pathways. In addition, the second freeze-casting and freeze-drying process involving the BN−PU aqueous dispersion effectively eliminated the transverse rGO−PU bridges connecting the rGO−PU layers (Figure 5a) by the growth of ice crystals, leading to lower electrical conductivities and thus suppressed dielectric losses of the microlaminate composites.

The dielectric properties obtained at 1 kHz along with the corresponding $U_{\max}$ calculated using eq 2 are summarized in Figure 5e,f. An excellent dielectric constant of 1084 was recorded by the rGO−PU/BN−PU_1.38 composites with a low loss of 0.091. Practically viable dielectric losses lower than 0.1 were achieved for all combinations of rGO−PU and BN−PU hybrids in this study, confirming the microlaminate structure as a promising choice for developing high-performance dielectric materials. Three different batches of materials were used for the same fabrication process and testing procedure to confirm the reproducibility of the results, as shown in Figures 5e,f and S9.

Further, the dielectric strength of rGO−PU/BN−PU_0.67 microlaminate composites was enhanced to a maximum value of 95.1 MV/m, almost 18 times that of the neat rGO−PU composite without the BN−PU barrier layers (Figure 5f and Table S1). The BN−PU layer's inherently high dielectric strength of 283 MV/m and their barrier effect on the electrical conduction among the rGO−PU layers contributed to this ameliorating trait. The energy densities of the neat PU and the rGO−PU composites were almost negligible with ultralow values of less than 1 J/cm^3. The incorporation of 3.85 vol % BN nanosheets in PU resulted in an increase of 2.8-folds that of the neat PU, which is consistent with previous study.[11] Although the rGO−PU/BN−PU microlaminate composites delivered lower dielectric constants than the rGO−PU composites and lower dielectric strengths than the neat PU or 3.85 vol % BN−PU, the microlaminate composites exhibited significantly higher $U_{\max}$ than the neat PU, rGO−PU, or BN−PU acting alone. A highest value of 22.7 J/cm^3 was achieved by the rGO−PU/BN−PU_0.67 composites, which is 12, 36, and 43 times higher than those of the 3.85 vol % BN−PU composite, neat PU, and the 0.73 vol % rGO−PU composite. The above observation means that the dielectric constant, dielectric loss, and dielectric strength have to be balanced to achieve optimized energy densities of composites. In summary, the high energy densities of GO−PU/BN−PU microlaminate composites are attributed to several ameliorating factors, including (i) high dielectric constants arising from

DOI: 10.1021/acsami.8b08031
ACS Appl. Mater. Interfaces 2018, 10, 26641−26652

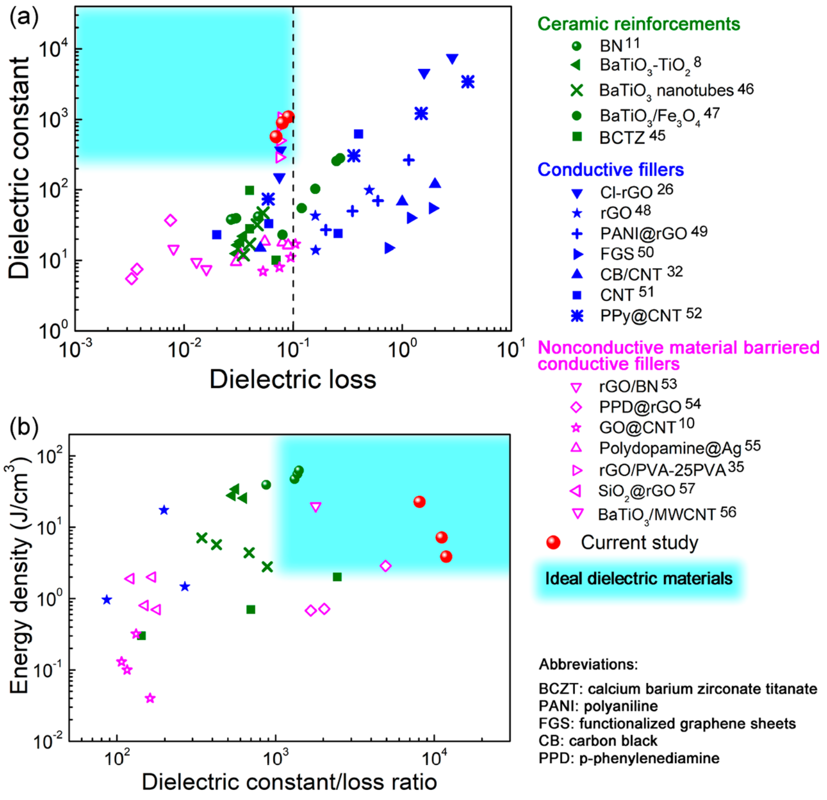

Figure 6. Comparison of dielectric performance between rGO−PU/BN−PU microlaminate composites and other polymer-based composites: (a) dielectric constant as a function of dielectric loss and (b) energy density as a function of dielectric constant/loss ratio.

the rGO−PU layers; (ii) significantly suppressed leakage currents in the transverse direction and thus low dielectric losses, thanks to the electrically insulating BN−PU layers among the rGO−PU layers; (iii) the microlaminate structure with a blocking effect of leakage currents in the thickness direction; and (iv) intrinsically high dielectric strengths of the BN−PU layers.

The excellent dielectric properties and energy densities of the rGO−PU/BN−PU microlaminate structure are compared with those of composites reinforced with different types of fillers, as shown in Figure 6. Figure 6a indicates that the composites reinforced with high-*k* inorganic fillers deliver relatively low dielectric losses due to their intrinsically insulating characteristics, but their dielectric constants are limited even at high filler loadings.[8,45−47] Dielectric losses lower than 0.1, an important criterion for practical applications, were achieved using high-*k* ceramic fillers, such as $BaTiO_3$ and BCZT. The addition of BN reduced the dielectric constants of polymers due to its intrinsically low dielectric constant, whereas the dielectric losses were well suppressed.[11] The dielectric constants of the polymer composites were greatly improved after adding highly conductive reinforcements, such as CNTs and graphene, but at the expense of much higher dielectric losses. The encapsulation of conductive fillers by insulating polymers and/or combining conductive fillers with inorganic fillers were proven to be effective in maintaining both high dielectric constants and restrained dielectric losses.[26,32,48−52] Thanks to the insulating layers on the conductive filler surface, extremely low dielectric losses lower than 0.01 were achieved, but the enhancement of the dielectric constants remained inadequate.[10,53−56] A recent breakthrough using neat poly(vinyl alcohol) (PVA) as the barrier layers among conductive rGO/PVA delivered a remarkable dielectric constant of 1059 and a loss of ∼0.8, although the energy density was not measured.[35] The current rGO−PU/BN−PU composites with a microlaminate structure where the electrically insulating BN−PU barriers isolate the conductive rGO−PU layers presented a combination of excellent dielectric constants as high as 1084 and a low dielectric loss of 0.091, making them highly competitive for real-world applications.

The energy densities of the microlaminate composites are also proven to be among the highest in a plot against the dielectric constant/loss ratio, as shown in Figure 6b. For the polymer composites containing dispersed conductive fillers, it is challenging to achieve both high dielectric constant/loss ratio and high energy density because of their relatively high dielectric losses.[48] High-*k* ceramic/polymer composites generally outperform conductive polymer composites owing to the intrinsically high dielectric strengths and low dielectric losses of high-*k* ceramics.[8,45,46] However, relatively high filler loadings are necessary to obtain optimized dielectric performances, inevitably sacrificing the light weight and the mechanical properties of polymer-based composites. BN has been verified to be a promising high-*k* ceramic with a high energy density,[11] but the dielectric constant/loss ratio is low because of its low dielectric constant. The isolation of conductive fillers with an insulating material makes it possible to obtain both high dielectric constant/loss ratios and relatively high energy densities.[10,53,54,57] The rationally designed rGO−PU/BN−PU composites in this study revealed such desirable attributes simultaneously. In summary, Figure 6a,b clearly demonstrate the benefits of the microlaminate structure consisting of alternating high-*k* and high-E_b layers for emerging dielectric applications.

4. CONCLUSIONS

Highly aligned microlaminate composites consisting of alternating rGO−PU and BN−PU layers were fabricated by a two-step freeze-casting/drying process where the aligned rGO−PU aerogel was infiltrated with the BN−PU aqueous dispersion, followed by compaction. The transverse conductive bridges connecting the longitudinal rGO−PU aerogel skeleton were effectively broken by the electrically insulating BN−PU layers, resulting in significantly enhanced dielectric properties. The following can be highlighted from this study:

(i) Highly aligned rGO−PU aerogels with conductive bridges among the neighboring rGO−PU layers were fabricated by freeze casting. The polydopamine-functionalized rGO were uniformly dispersed in the PU matrix, leading to an excellent dielectric constant of 4258 with a moderate dielectric loss of 3.2 for the 0.73 vol % rGO−PU. However, the highly enhanced dielectric constant of the composite was at the expense of a sharply reduced dielectric strength of PU from 120 to 5.3 MV/m, resulting in a concomitant reduction in energy density by almost 75%.

(ii) BN nanosheets with an average diameter of 0.39 μm and an average layer number of 3.9 were synthesized using a urea-assisted ball-milling method. The BN−PU composite dispersion was intercalated to break the conducting bridges connecting the rGO−PU composite skeleton during the second freeze-casting/drying routine.

(iii) The microlaminate composites consisting of highly aligned alternating rGO−PU and BN−PU layers were formed after compaction. The dielectric constants of the microlaminate composites remained as high as 1084, whereas their losses were drastically suppressed to below 0.1. The dielectric strengths and energy densities were restored in the microlaminate composites, achieving an energy density of 22.7 J/cm^3, which is 36 and 43 times higher than those of the neat PU and the 0.73 vol % rGO−PU composites, respectively. The longitudinally conductive, transversely insulating high-k rGO−PU layers and the high-E_b BN−PU layers were mainly responsible for the excellent dielectric properties and high energy densities.

■ ASSOCIATED CONTENT

Supporting Information

The Supporting Information is available free of charge on the ACS Publications website at DOI: 10.1021/acsami.8b08031.

SEM image of GO sheets; freeze-casting apparatus; XPS, XRD; morphologies of rGO−PU composites; schematic comparison of unidirectional and bidirectional freeze casting; dielectric properties (PDF)

■ AUTHOR INFORMATION

Corresponding Author

*E-mail: mejkkim@ust.hk.

ORCID

Xi Shen: 0000-0003-1688-4931

Jang-Kyo Kim: 0000-0002-5390-8763

Notes

The authors declare no competing financial interest.

■ ACKNOWLEDGMENTS

This project was financially supported by the Research Grants Council of Hong Kong SAR (GRF Projects: 16203415, 16229216, and 16205517). Technical assistance from the Department of Electronic and Computer Engineering (Prof. Philip K. T. Mok), the Materials Characterization and Preparation Facilities (MCPF), and the Advanced Engineering Material Facility (AEMF) is appreciated.

■ REFERENCES

(1) Hu, P.; Shen, Y.; Guan, Y.; Zhang, X.; Lin, Y.; Zhang, Q.; Nan, C.-W. Topological-Structure Modulated Polymer Nanocomposites Exhibiting Highly Enhanced Dielectric Strength and Energy Density. *Adv. Funct. Mater.* **2014**, *24*, 3172−3178.

(2) Kim, P.; Jones, S. C.; Hotchkiss, P. J.; Haddock, J. N.; Kippelen, B.; Marder, S. R.; Perry, J. W. Phosphonic Acid-Modified Barium Titanate Polymer Nanocomposites with High Permittivity and Dielectric Strength. *Adv. Mater.* **2007**, *19*, 1001−1005.

(3) Yuan, J.-K.; Dang, Z.-M.; Yao, S.-H.; Zha, J.-W.; Zhou, T.; Li, S.-T.; Bai, J. Fabrication and Dielectric Properties of Advanced High Permittivity Polyaniline/Poly (vinylidene fluoride) Nanohybrid Films with High Energy Storage Density. *J. Mater. Chem.* **2010**, *20*, 2441−2447.

(4) Yousefi, N.; Sun, X.; Lin, X.; Shen, X.; Jia, J.; Zhang, B.; Tang, B.; Chan, M.; Kim, J.-K. Highly Aligned Graphene/Polymer Nanocomposites with Excellent Dielectric Properties for High-performance Electromagnetic Interference Shielding. *Adv. Mater.* **2014**, *26*, 5480−5487.

(5) Yu, C.-R.; Wu, D.-M.; Liu, Y.; Qiao, H.; Yu, Z.-Z.; Dasari, A.; Du, X.-S.; Mai, Y.-W. Electrical and Dielectric Properties of Polypropylene Nanocomposites Based on Carbon Nanotubes and Barium Titanate Nanoparticles. *Compos. Sci. Technol.* **2011**, *71*, 1706−1712.

(6) Yang, W.; Yu, S.; Sun, R.; Du, R. Nano- and Microsize Effect of CCTO Fillers on the Dielectric Behavior of CCTO/PVDF Composites. *Acta Mater.* **2011**, *59*, 5593−5602.

(7) Ke, S.; Lin, P.; Zeng, X.; Huang, H.; Zhou, L.; Mai, Y.-W. Tuning of Dielectric and Ferroelectric Properties in Single Phase $BiFeO_3$ Ceramics with Controlled Fe^{2+}/Fe^{3+} Ratio. *Ceram. Int.* **2014**, *40*, 5263−5268.

(8) Zhang, X.; Shen, Y.; Zhang, Q.; Gu, L.; Hu, Y.; Du, J.; Lin, Y.; Nan, C.-W. Ultrahigh Energy Density of Polymer Nanocomposites Containing $BaTiO_3@TiO_2$ Nanofibers by Atomic-Scale Interface Engineering. *Adv. Mater.* **2015**, *27*, 819−824.

(9) Shen, Y.; Lin, Y.; Li, M.; Nan, C.-W. High Dielectric Performance of Polymer Composite Films Induced by A Percolating Interparticle Barrier Layer. *Adv. Mater.* **2007**, *19*, 1418−1422.

(10) Wu, C.; Huang, X.; Wu, X.; Xie, L.; Yang, K.; Jiang, P. Graphene Oxide-Encapsulated Carbon Nanotube Hybrids for High Dielectric Performance Nanocomposites with Enhanced Energy Storage Density. *Nanoscale* **2013**, *5*, 3847−3855.

(11) Li, Q.; Zhang, G.; Liu, F.; Han, K.; Gadinski, M. R.; Xiong, C.; Wang, Q. Solution-Processed Ferroelectric Terpolymer Nanocomposites with High Breakdown Strength and Energy Density Utilizing Boron Nitride Nanosheets. *Energy Environ. Sci.* **2015**, *8*, 922−931.

(12) Li, Q.; Han, K.; Gadinski, M. R.; Zhang, G.; Wang, Q. High Energy and Power Density Capacitors from Solution-Processed Ternary Ferroelectric Polymer Nanocomposites. *Adv. Mater.* **2014**, *26*, 6244−6249.

(13) Li, Q.; Chen, L.; Gadinski, M. R.; Zhang, S.; Zhang, G.; Li, H. U.; Iagodkine, E.; Haque, A.; Chen, L.-Q.; Jackson, T. N.; Wang, Q. Flexible High-Temperature Dielectric Materials from Polymer Nanocomposites. *Nature* **2015**, *523*, 576−579.

(14) Li, Q.; Liu, F.; Yang, T.; Gadinski, M. R.; Zhang, G.; Chen, L.-Q.; Wang, Q. Sandwich-Structured Polymer Nanocomposites with High Energy Density and Great Charge−Discharge Efficiency at Elevated Temperatures. *Proc. Natl. Acad. Sci. U.S.A.* **2016**, 9995.

(15) Lin, X.; Shen, X.; Zheng, Q.; Yousefi, N.; Ye, L.; Mai, Y.-W.; Kim, J.-K. Fabrication of Highly-Aligned, Conductive, and Strong Graphene Papers Using Ultralarge Graphene Oxide Sheets. *ACS Nano* **2012**, *6*, 10708−10719.

(16) Jia, J.; Kan, C.-M.; Lin, X.; Shen, X.; Kim, J.-K. Effects of Processing and Material Parameters on Synthesis of Monolayer Ultralarge Graphene Oxide Sheets. *Carbon* **2014**, *77*, 244−254.

(17) Xu, L. Q.; Yang, W. J.; Neoh, K.-G.; Kang, E.-T.; Fu, G. D. Dopamine-Induced Reduction and Functionalization of Graphene Oxide Nanosheets. *Macromolecules* **2010**, *43*, 8336−8339.

(18) Wang, Z.; Shen, X.; Han, N. M.; Liu, X.; Wu, Y.; Ye, W.; Kim, J.-K. Ultralow Electrical Percolation in Graphene Aerogel/Epoxy Composites. *Chem. Mater.* **2016**, *28*, 6731−6741.

(19) Bai, H.; Chen, Y.; Delattre, B.; Tomsia, A. P.; Ritchie, R. O. Bioinspired Large-scale Aligned Porous Materials Assembled with Dual Temperature Gradients. *Sci. Adv.* **2015**, *1*, No. e1500849.

(20) Lei, W.; Mochalin, V. N.; Liu, D.; Qin, S.; Gogotsi, Y.; Chen, Y. Boron Nitride Colloidal Solutions, Ultralight Aerogels and Freestanding Membranes Through One-Step Exfoliation and Functionalization. *Nat. Commun.* **2015**, *6*, No. 8849.

(21) Wang, Z.; Shen, X.; Akbari Garakani, M.; Lin, X.; Wu, Y.; Liu, X.; Sun, X.; Kim, J. K. Graphene Aerogel/Epoxy Composites with Exceptional Anisotropic Structure and Properties. *ACS Appl. Mater. Interfaces* **2015**, *7*, 5538−5549.

(22) Lee, W.; Lee, J. U.; Jung, B. M.; Byun, J.-H.; Yi, J.-W.; Lee, S.-B.; Kim, B.-S. Simultaneous Enhancement of Mechanical, Electrical and Thermal Properties of Graphene Oxide Paper by Embedding Dopamine. *Carbon* **2013**, *65*, 296−304.

(23) Kaminska, I.; Das, M. R.; Coffinier, Y.; Niedziolka-Jonsson, J.; Sobczak, J.; Woisel, P.; Lyskawa, J.; Opallo, M.; Boukherroub, R.; Szunerits, S. Reduction and Functionalization of Graphene Oxide Sheets Using Biomimetic Dopamine Derivatives in One Step. *ACS Appl. Mater. Interfaces* **2012**, *4*, 1016−1020.

(24) Zhang, Z.; Zhang, J.; Zhang, B.; Tang, J. Mussel-Inspired Functionalization of Graphene for Synthesizing Ag-Polydopamine-Graphene Nanosheets as Antibacterial Materials. *Nanoscale* **2013**, *5*, 118−123.

(25) Shen, X.; Wang, Z.; Wu, Y.; Liu, X.; Kim, J.-K. Effect of Functionalization on Thermal Conductivities of Graphene/Epoxy Composites. *Carbon* **2016**, *108*, 412−422.

(26) Wu, Y.; Lin, X. Y.; Shen, X.; Sun, X. Y.; Liu, X.; Wang, Z. Y.; Kim, J.-K. Exceptional Dielectric Properties of Chlorine-Doped Graphene Oxide/Poly (vinylidene fluoride) Nanocomposites. *Carbon* **2015**, *89*, 102−112.

(27) Shehzad, K.; Xu, Y.; Gao, C.; Duan, X. Three-Dimensional Macro-Structures of Two-Dimensional Nanomaterials. *Chem. Soc. Rev.* **2016**, *45*, 5541−5588.

(28) Yousefi, N.; Lin, X.; Zheng, Q.; Shen, X.; Pothnis, J. R.; Jia, J.; Zussman, E.; Kim, J.-K. Simultaneous in situ Reduction, Self-Alignment and Covalent Bonding in Graphene Oxide/Epoxy Composites. *Carbon* **2013**, *59*, 406−417.

(29) Moniruzzaman, M.; Winey, K. I. Polymer Nanocomposites Containing Carbon Nanotubes. *Macromolecules* **2006**, *39*, 5194−5205.

(30) Shehzad, K.; Dang, Z.-M.; Ahmad, M. N.; Sagar, R. U. R.; Butt, S.; Farooq, M. U.; Wang, T.-B. Effects of Carbon Nanotubes Aspect Ratio on the Qualitative and Quantitative Aspects of Frequency Response of Electrical Conductivity and Dielectric Permittivity in the Carbon Nanotube/Polymer Composites. *Carbon* **2013**, *54*, 105−112.

(31) Su, Q.; Pang, S.; Alijani, V.; Li, C.; Feng, X.; Müllen, K. Composites of Graphene with Large Aromatic Molecules. *Adv. Mater.* **2009**, *21*, 3191−3195.

(32) Shehzad, K.; Xu, Y.; Gao, C.; Li, H.; Dang, Z.-M.; Hasan, T.; Luo, J.; Duan, X. Flexible Dielectric Nanocomposites with Ultrawide Zero-Temperature Coefficient Windows for Electrical Energy Storage and Conversion under Extreme Conditions. *ACS Appl. Mater. Interfaces* **2017**, *9*, 7591−7600.

(33) Shang, J.; Zhang, Y.; Yu, L.; Luan, X.; Shen, B.; Zhang, Z.; Lv, F.; Chu, P. K. Fabrication and Enhanced Dielectric Properties of Graphene−Polyvinylidene Fluoride Functional Hybrid Films with A Polyaniline Interlayer. *J. Mater. Chem. A* **2013**, *1*, 884−890.

(34) Yang, K.; Huang, X.; Fang, L.; He, J.; Jiang, P. Fluoro-Polymer Functionalized Graphene for Flexible Ferroelectric Polymer-Based High-k Nanocomposites with Suppressed Dielectric Loss and Low Percolation Threshold. *Nanoscale* **2014**, *6*, 14740−14753.

(35) Wang, Z.; Han, N. M.; Wu, Y.; Liu, X.; Shen, X.; Zheng, Q.; Kim, J.-K. Ultrahigh Dielectric Constant and Low Loss of Highly-Aligned Graphene Aerogel/Poly(vinyl alcohol) Composites with Insulating Barriers. *Carbon* **2017**, *123*, 385−394.

(36) Zhou, K. G.; Mao, N. N.; Wang, H. X.; Peng, Y.; Zhang, H. L. A Mixed-Solvent Strategy for Efficient Exfoliation of Inorganic Graphene Analogues. *Angew. Chem.* **2011**, *123*, 11031−11034.

(37) Zhu, W.; Gao, X.; Li, Q.; Li, H.; Chao, Y.; Li, M.; Mahurin, S. M.; Li, H.; Zhu, H.; Dai, S. Controlled Gas Exfoliation of Boron Nitride into Few-Layered Nanosheets. *Angew. Chem.* **2016**, *128*, 10924−10928.

(38) Zeng, Z.; Sun, T.; Zhu, J.; Huang, X.; Yin, Z.; Lu, G.; Fan, Z.; Yan, Q.; Hng, H. H.; Zhang, H. An Effective Method for the Fabrication of Few-Layer-Thick Inorganic Nanosheets. *Angew. Chem., Int. Ed.* **2012**, *51*, 9052−9056.

(39) Du, M.; Li, X.; Wang, A.; Wu, Y.; Hao, X.; Zhao, M. One-Step Exfoliation and Fluorination of Boron Nitride Nanosheets and A Study of Their Magnetic Properties. *Angew. Chem.* **2014**, *126*, 3719−3723.

(40) Lin, Y.; Connell, J. W. Advances in 2D Boron Nitride Nanostructures: Nanosheets, Nanoribbons, Nanomeshes, and Hybrids with Graphene. *Nanoscale* **2012**, *4*, 6908−6939.

(41) Zhao, G.; Zhang, F.; Wu, Y.; Hao, X.; Wang, Z.; Xu, X. One-Step Exfoliation and Hydroxylation of Boron Nitride Nanosheets with Enhanced Optical Limiting Performance. *Adv. Opt. Mater.* **2016**, *4*, 141−146.

(42) Gorbachev, R. V.; Riaz, I.; Nair, R. R.; Jalil, R.; Britnell, L.; Belle, B. D.; Hill, E. W.; Novoselov, K. S.; Watanabe, K.; Taniguchi, T.; et al. Hunting for Monolayer Boron Nitride: Optical and Raman Signatures. *Small* **2011**, *7*, 465−468.

(43) Arenal, R.; Ferrari, A.; Reich, S.; Wirtz, L.; Mevellec, J.-Y.; Lefrant, S.; Rubio, A.; Loiseau, A. Raman Spectroscopy of Single-Wall Boron Nitride Nanotubes. *Nano Lett.* **2006**, *6*, 1812−1816.

(44) Lee, D.; Lee, B.; Park, K. H.; Ryu, H. J.; Jeon, S.; Hong, S. H. Scalable Exfoliation Process for Highly Soluble Boron Nitride Nanoplatelets by Hydroxide-Assisted Ball Milling. *Nano Lett.* **2015**, *15*, 1238−1244.

(45) Luo, B.; Wang, X.; Wang, Y.; Li, L. Fabrication, Characterization, Properties and Theoretical Analysis of Ceramic/PVDF Composite Flexible Films with High Dielectric Constant and Low Dielectric Loss. *J. Mater. Chem. A* **2014**, *2*, 510−519.

(46) Pan, Z.; Yao, L.; Zhai, J.; Shen, B.; Wang, H. Significantly Improved Dielectric Properties and Energy Density of Polymer Nanocomposites via Small Loaded of $BaTiO_3$ Nanotubes. *Compos. Sci. Technol.* **2017**, *147*, 30−38.

(47) Zhang, C.; Chi, Q.; Dong, J.; Cui, Y.; Wang, X.; Liu, L.; Lei, Q. Enhanced Dielectric Properties of Poly (vinylidene fluoride) Composites Filled with Nano Iron Oxide-Deposited Barium Titanate Hybrid Particles. *Sci. Rep.* **2016**, *6*, No. 33508.

(48) Yang, C.; Hao, S.-J.; Dai, S.-L.; Zhang, X.-Y. Nanocomposites of Poly (vinylidene fluoride)-Controllable Hydroxylated/Carboxylated Graphene with Enhanced Dielectric Performance for Large Energy Density Capacitor. *Carbon* **2017**, *117*, 301−312.

(49) Maity, N.; Mandal, A.; Nandi, A. K. Hierarchical Nanostructured Polyaniline Functionalized Graphene/Poly (vinylidene fluoride) Composites for Improved Dielectric Performances. *Polymer* **2016**, *103*, 83−97.

(50) Li, C.-Q.; Zha, J.-W.; Long, H.-Q.; Wang, S.-J.; Zhang, D.-L.; Dang, Z.-M. Mechanical and Dielectric Properties of Graphene Incorporated Polypropylene Nanocomposites Using Polypropylene-graft-maleic Anhydride as A Compatibilizer. *Compos. Sci. Technol.* **2017**, *153*, 111−118.

(51) Sun, H.; Zhang, H.; Liu, S.; Ning, N.; Zhang, L.; Tian, M.; Wang, Y. Interfacial Polarization and Dielectric Properties of Aligned Carbon Nanotubes/Polymer Composites: The Role of Molecular Polarity. *Compos. Sci. Technol.* **2018**, *154*, 145−153.

(52) He, Z.-Z.; Yu, X.; Yang, J.-H.; Zhang, N.; Huang, T.; Wang, Y.; Zhou, Z.-W. Largely Enhanced Dielectric Properties of Poly (vinylidene fluoride) Composites Achieved by Adding Polypyrrole-Decorated Graphene Oxide. *Composites, Part A* **2018**, *104*, 89−100.

(53) Wu, K.; Lei, C.; Yang, W.; Chai, S.; Chen, F.; Fu, Q. Surface Modification of Boron Nitride by Reduced Graphene Oxide for Preparation of Dielectric Material with Enhanced Dielectric Constant and Well-Suppressed Dielectric Loss. *Compos. Sci. Technol.* **2016**, *134*, 191−200.

(54) Fang, X.; Liu, X.; Cui, Z.-K.; Qian, J.; Pan, J.; Li, X.; Zhuang, Q. Preparation and Properties of Thermostable Well-Functionalized Graphene Oxide/Polyimide Composite Films with High Dielectric Constant, Low Dielectric Loss and High Strength via in situ Polymerization. *J. Mater. Chem. A* **2015**, *3*, 10005−10012.

(55) Hu, D.; Jiang, M.; Hou, Y.; Zhang, J.; Fang, D.; Liu, L.; Huang, J.; Li, H.; Xiong, C. Dielectric Loss Suppression of Silver/Poly (vinylidene fluoride) Composite Films with Polydopamine. *J. Macromol. Sci., Part B: Phys.* **2018**, *57*, 255−265.

(56) Jin, Y.; Xia, N.; Gerhardt, R. A. Enhanced Dielectric Properties of Polymer Matrix Composites with $BaTiO_3$ and MWCNT Hybrid Fillers Using Simple Phase Separation. *Nano Energy* **2016**, *30*, 407−416.

(57) Han, K.; Li, Q.; Chen, Z.; Gadinski, M. R.; Dong, L.; Xiong, C.; Wang, Q. Suppression of Energy Dissipation and Enhancement of Breakdown Strength in Ferroelectric Polymer-Graphene Percolative Composites. *J. Mater. Chem. C* **2013**, *1*, 7034−7042.